Journal of Power Sources 196 (2011) 5784–5791

Contents lists available at ScienceDirect

Journal of Power Sources

journal homepage: www.elsevier.com/locate/jpowsour

Liquid crystal based electrolyte with light trapping scheme for enhancing photovoltaic performance of quasi-solid-state dye-sensitized solar cells

Meng Wang, Xu Pan, Xiaqin Fang, Lei Guo, Changneng Zhang, Yang Huang, Zhipeng Huo, Songyuan Dai *

Key Laboratory of Novel Thin Film Solar Cells, Institute of Plasma Physics, Chinese Academy of Sciences, Hefei, 230031, PR China

ARTICLE INFO

Article history:
Received 9 September 2010
Received in revised form 18 February 2011
Accepted 19 February 2011
Available online 26 February 2011

Keywords:
Dye-sensitized
Solar cells
Liquid crystal
Light trapping
Quasi-solid-state

ABSTRACT

In this study, nematic liquid crystal, 4-Cyano-4′-n-heptyloxybiphenyl, is introduced into the poly(vinylidenefluoride-co-hexafluoropropylene) (PVDF) based polymeric gel electrolyte for quasi-solid-state dye-sensitized solar cells (DSC), aiming to improve the photovoltaic performance of DSC. The effects of liquid crystal on the electrochemical behavior of I_3^-/I^- and photovoltaic performance, dynamic response as well as long-term stability of DSC are studied in detail. It is found that although the addition of liquid crystal would hinder the charge transport in the electrolyte, it could still fulfill the requirements of the photocurrent for DSC. More important, a significant increase in the photocurrent density for DSC is observed when liquid crystal is introduced into PVDF based polymeric gel electrolyte, resulting in the higher photoelectric conversion efficiency. The large increase in short-circuit photocurrent density could be attributed to the higher light harvesting efficiency, which is caused by the effective formation of light trapping scheme in electrolyte due to the addition of liquid crystal. Besides, at-rest long-term stability shows that when liquid crystal is introduced into PVDF based polymeric gel electrolyte, DSC could retain over 92% of its initial photoelectric conversion efficiency value after 1000 h, exhibiting relatively better stability.

1. Introduction

During the past decades, dye-sensitized solar cells (DSC) are attracting widespread academic and commercial interest for the conversion of sunlight into electricity due to their low cost, easy fabrication and high efficiency [1]. An impressive photoelectric conversion efficiency over 11% has been obtained [2,3] for the photoelectric device with conventional liquid electrolyte. Unfortunately, the presence of the liquid electrolyte may result in some practical limitation including leakage evaporation, sealing difficulties and electrode corrosion [4,5]. Therefore numerous efforts have been made to replace the liquid electrolyte to improve the stability of the DSC such as ionic liquids [6], hole conductors [7]. However, the photovoltaic performance of DSC with ionic liquids or all-solid-state electrolyte as electrolyte is still too low for practical application. Recently, quasi-solid state electrolyte based on nanocomposite [8], low molecular organgelator [9], and polymer material [10,11] incorporating I_3^-/I^- have received much attention. Among those, the quasi-solid-state electrolyte based on poly(vinylidenefluoride-co-hexafluoropropylene) (PVDF) have attracted the greatest interest due to its high stability and relatively high photoelectric conversion efficiency for DSC [12]. However, gelation of liquid electrolyte may exert negative effect on the photovoltaic performance of DSC. Therefore, numerous researches have been focused on improving the photovoltaic performance of quasi-solid-state DSC.

Liquid crystals (LC), as the fourth state matter combining properties of liquids and solids [13], are usually used as the media for the organic catalytic synthesis [14], functional nanostructured materials [15] and polymer dispersed liquid crystals (PDLCs) displays due to its light scattering property [16]. In recent days, a few studies have shown that the introduction of liquid crystal into the electrolyte for the DSC would enhance the ion conductivity and thus the photovoltaic performance of the DSC [17,18]. Kim et al. [19,20] has successfully introduced the liquid crystals E7 and ML-0249 into the polyacrylonitrile (PAN) based polymer electrolyte to improve the ion conductivity and therefore the short-circuit current density of the DSC. However, reports about the application of LC in DSC are still limited. Besides, few have been reported about the light scattering property when LC is introduced into the polymeric electrolyte and its influence on the photovoltaic performance of DSC.

In this paper, the nematic liquid crystal, 4-Cyano-4′-n-heptyloxybiphenyl (Fig. 1), was introduced into the PVDF based polymeric gel electrolyte for quasi-solid-state DSC and some good results were obtained. The light trapping scheme was confirmed in

* Corresponding author. Tel.: +86 551 5591377; fax: +86 551 5591377.
E-mail address: sydai@ipp.ac.cn (S. Dai).

0378-7753/$ – see front matter © 2011 Elsevier B.V. All rights reserved.
doi:10.1016/j.jpowsour.2011.02.051

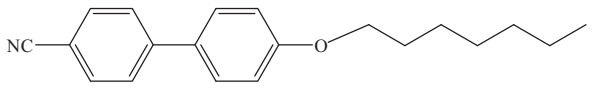

Fig. 1. Molecular structure of nematic liquid crystal, 4-Cyano-4′-n-heptyloxybiphenyl.

the electrolyte due to the addition of liquid crystal and its effects on the performance, dynamic response as well as at-rest long-term stability were also studied in detail.

2. Experimental

2.1. Materials

Anhydrous lithium iodide, iodine, 1-methylbenzimidazole (NMBI), and acetonitrile (ACN) were purchased from Fluka. The nematic liquid crystal, 4-Cyano-4′-n-heptyloxybiphenyl, was obtained from Alfa. All the chemical reagents were used as received. 1-propyl-3-methylimidazolium iodide (MPII) was synthesized by the quaternization of 1-methylimidazole and 1-iodopropane and its purity has been confirmed by ^{1}H NMR.

2.2. Preparation of electrolytes

Two different electrolytes were used. The PVDF based polymeric gel electrolyte was prepared by adding 10 wt% PVDF (versus liquid electrolyte) into liquid electrolyte, which consisted of 0.1 mol L^{-1} iodine, 1.0 mol L^{-1} MPII, 0.45 mol L^{-1} NMBI and 0.1 mol L^{-1} lithium iodide in acetonitrile, and then stirred vigorously at 80 °C for 24 h to ensure homogeneity. After cooling down to room temperature, the PVDF based polymeric gel electrolyte was formed (denoted as A). The liquid crystal (LC) and PVDF based electrolyte was prepared the same as electrolyte A by adding 20 wt % nematic liquid crystal 4-Cyano-4′-n-heptyloxybiphenyl into PVDF based polymeric gel electrolyte A (denoted as B) (Fig. 2).

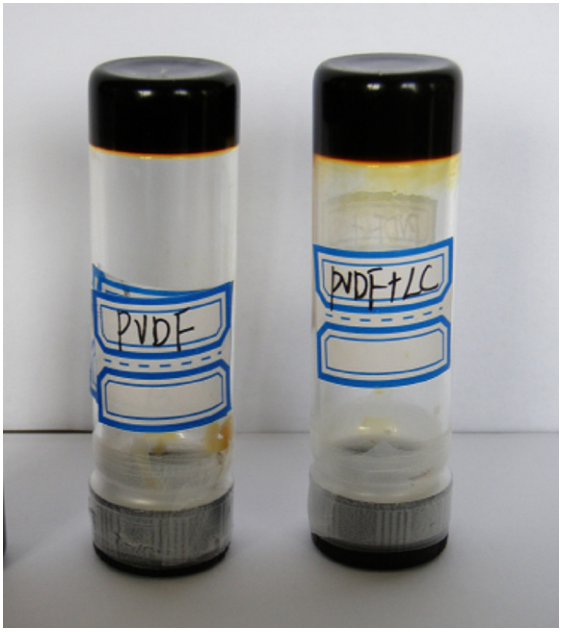

Fig. 2. Photographs of the PVDF based polymeric gel electrolyte A and liquid crystal and PVDF based electrolyte B from left to right. The bottles are upside down.

2.3. Fabrication of DSC

DSC was assembled in a sandwich configuration as reported previously [21,22]. The colloidal TiO_2 nanoparticles were prepared by hydrolysis of titanium tetraisopropoxide as described elsewhere [23]. Nanocrystalline electrodes about 10 μm in thickness were obtained by screen-printing TiO_2 paste on FTO glass (TEC-8, LOF) and then sintering at 450 °C for 30 min in air. The photoelectrodes were immersed into dye solution containing C106 (0.3 mM) [3] in a mixture of acetonitrile and *tert*-butyl alcohol (volume ratio: 1/1) at room temperature for 12 h. The platinized counter electrodes were obtained by spraying H_2PtCl_6 solution to FTO glass followed by heating at 410 °C for 20 min. Then, the counter electrode was placed directly on the top of the dyed TiO_2 film sealed with thermal adhesive films (Surlyn, Dupont). And the electrolyte was filled from a hole made on the counter electrode, which was later sealed by a cover glass and thermal adhesive films.

2.4. Measurements

Steady-state voltammetry of the electrolytes were adopted in a conventional electrochemical cell equipped with a 1.0 μm platinum ultra-microelectrode (CHI107) as working electrode, and with a 1 mm radius platinum disk electrode (CHI102) as counter electrode and reference electrode. A slow scan rate of 5 mV s^{-1} was used in order to obtain steady-state current–voltage curves. This work was carried out at 25 °C on an electrochemical workstation (CHI660A, CH Instruments Inc., Austin, TX). Ion conductivity measurements were carried out using two electrodes thin-layer cells according to previous report [24]. The conductivity of the electrolytes was measured by using a frequency response analyzer equipped with a potentiostat (IM6e, Zahner, Germany) at 0 V bias in the frequency range from 1 Hz to 1000 kHz with modulation amplitude of 10 mV. Conductivity of the electrolytes was determined from the high frequency intercept with the real axis in the Nyquist plot by using the following equation [25]

$$\sigma = \frac{L}{AR_b} \quad (1)$$

where σ is the conductivity of the electrolyte, L is the distance between the two electrode, A is the area of the electrodes, and R_b is the real resistance of the electrolyte estimated from the resistance Z' at which the resistance Z'' had its minimum value.

The photovoltaic performances of the DSC were measured by a Keithley 2420 3A source meter controlled by Testpoint software under solar simulator (solar AAA simulator, oriel USA, calibrated with a standard crystalline silicon solar). The total covered active electrode area with black mask of DSC was 0.16 cm^2. IPCE measurement was performed on QE/IPCE Measurement Kit (Newport, USA). Under full computer control, light from a 300 W xenon lamp was focused through a monochromator onto the solar cell under test. A computer-controlled monochrometer (74125 Oriel Cornerstone 260 1/4m Monochromator) was incremented through the spectral range (300–900 nm) to generate a photocurrent action spectra with a sampling interval of 10 nm and a current sampling time of 2 s. Light intensity of monochromatic light and the photocurrent generated on the solar cell were determined with 2931-C dual channel power meter and the 71675 calibrated UV silicon photodetector. All the components and the measurement process was fully automated using Oriel® Tracq Basic V5.0 software. The electron transport and recombination properties were measured by intensity-modulated photocurrent spectroscopy (IMPS) and intensity-modulated photovoltage spectroscopy (IMVS). IMPS/IMVS measurements were carried out on an IM6ex (Germany, Zahner Company) using light-emitting diodes (λ = 610 nm) driven by Expot (Germany, Zahner Company). The LED provided both dc and ac components of the

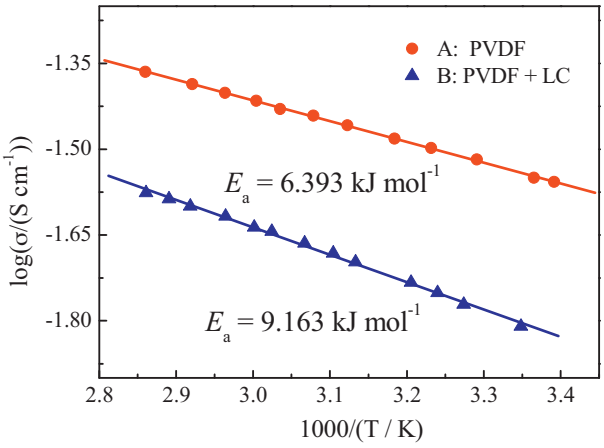

Fig. 3. The temperature dependences of the conductivity for the electrolyte A and electrolyte B.

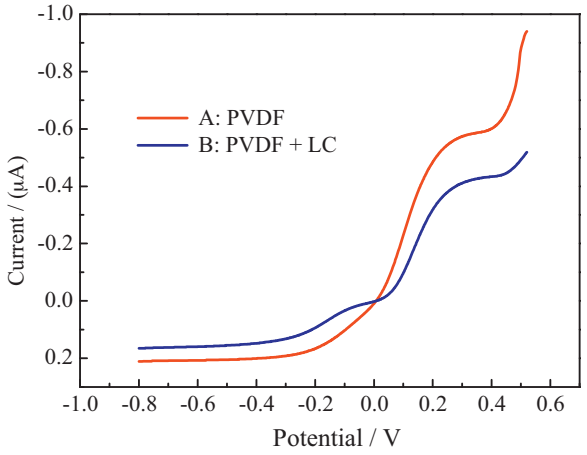

Fig. 4. The steady-state voltammograms of different electrolytes.

illumination. A small ac component was 10% or less than that of the dc component. The frequency range is 3 kHz to 0.1 Hz.

The transmittance and reflectance of the electrolyte and DSC were recorded on an ultraviolet-visible spectrophotometer (TU-1901, Persee Inc., China) equipped with a 16 mm diameter barium sulfate-coated integrating sphere in the range of 300–800 nm.

3. Results and discussion

3.1. Studies of the charge transfer in the electrolyte.

As the charge carrier, the transport of redox couple in the electrolyte would have a great effect on the performance of the DSC [26]. To characterize the influence of the liquid crystal on the transport of the redox couple in detail, the ion conductivity of the electrolyte was measured by impedance spectra. Fig. 3 shows the plots of the conductivity against $1/T$ for the different electrolytes. In all cases, the conductivity of electrolytes increases with the increase of the temperature due to the increase of the mobility of the ions in the electrolyte [27]. However the conductivity of the electrolyte B is lower than that of the PVDF based polymeric gel electrolyte A. According to Bhattacharya's viewpoint [28], the total conductivity of the electrolyte is given by the following relation

$$\sigma = nq\mu \tag{2}$$

where n is the number of dissociated charge carriers in the matrix, q is the charge carried by them, and μ is the mobility of the carriers. Therefore, any changes in the mobility of charge carriers will result in changing the total conductivity value. When the LC was added into the matrix of the polymeric gel electrolyte, it would cause the increase of the viscosity of the electrolyte [27], therefore the ions' mobility was decreased and consequently the conductivity of the electrolyte [29].

The temperature dependence of the conductivity shows a classical Arrhenius behavior according to the following equation

$$\sigma = \sigma_0 \exp\frac{-E_a}{RT} \tag{3}$$

where σ is the ionic conductivity, σ_0 is a constant, E_a is the activation energy, R is the gas constant and T is the temperature. The Arrhenius character of the conductivities in the given temperature range together ($R^2 > 0.995$) with the activation energies (9.167 and 6.393 kJ mol^{-1}) also suggests that the introduction of LC into the matrix of the polymeric electrolyte would hinder the mobility of the ions and decrease the ion conductivity of the electrolyte.

Further support is obtained by the steady-state voltammetry measurement, which was carried to obtain the diffusion controlled steady-state current of I_3^- and I^-. Fig. 4 shows the steady-state voltammograms of the electrolytes at 298 K, the apparent diffusion coefficients (D_{app}) of I_3^- and I^- ions were calculated from the anodic and cathodic steady-state current (I_{ss}) using the equation [24,30,31]

$$I_{ss} = 4nFD_{app}ca \tag{4}$$

here n is the electron number in the electrode reaction, F is the Faraday constant, and c is the bulk concentration of electroactive species, D_{app} is the apparent diffusion coefficient, a is the radius of the Pt ultramicroelectrode. The calculated results are listed in Table 1. From Fig. 4 and Table 1, it can be found that the D_{app} of I_3^- and I^- in electrolyte B (4.20 and 4.30×10^{-6} cm^2 s^{-1}) is lower than that in PVDF based polymeric gel electrolyte A (5.42 and 4.6×10^{-6} cm^2 s^{-1}), respectively, which may be associated with the decrease of the ion mobility as described above.

3.2. Studies of photovoltaic performance of the DSC with different electrolytes

Fig. 5 presents the photocurrent density–voltage characteristics of the DSC with electrolyte A and electrolyte B at AM 1.5 (one sun). The photoelectric conversion efficiency (η) and fill factor (FF) are evaluated using the following relations:

$$\eta = \frac{P_m}{P_{in}} = \frac{I_{sc} \times V_{OC} \times FF}{P_{in}} \tag{5}$$

$$FF = \frac{P_m}{I_{sc} \times V_{oc}} = \frac{I_m \times V_m}{I_{sc} \times V_{oc}} \tag{6}$$

where I_{sc} is the short-circuit photocurrent, V_{oc} is the open circuit photovoltage, P_m is the maximum output power, and P_{in} is the incident light power. I_m and V_m represent the maximum current and voltage, respectively. Table 2 summarizes the photovoltaic perfor-

Table 1
The steady-state current and the apparent diffusion coefficient of tri-iodide and iodide in different electrolytes.[a]

Electrolytes	I_{ss} (10^{-7} A)		D_{app} (10^{-6} cm^2 s^{-1})	
	I_3^-	I^-	I_3^-	I^-
PVDF	2.09	5.92	5.42	4.60
PVDF + LC	1.62	4.25	4.20	4.30

[a] Measured at 25 °C.

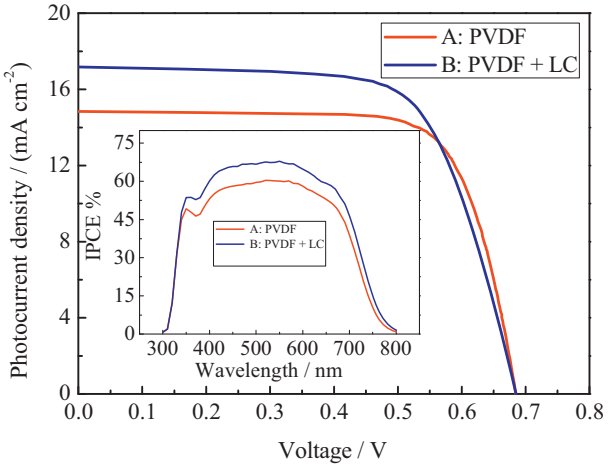

Fig. 5. *J–V* curves of the DSC with different electrolytes under 1 sun illumination. The insert is the photo action spectra of the DSC with different electrolyte. The aperture area of black mask: 0.16 cm^2.

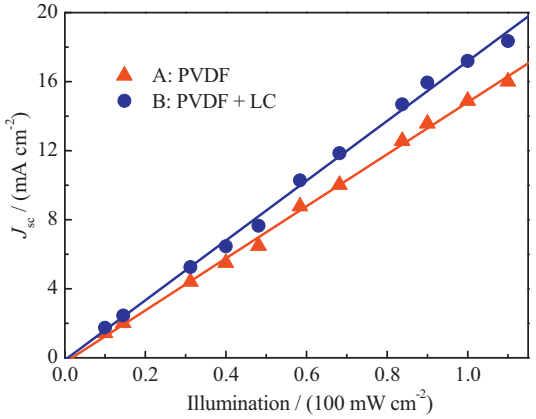

Fig. 6. The dependence of photocurrent density on illumination intensity.

mance parameters of dye-sensitized solar cells based on different electrolytes at AM 1.5.

From Fig. 5 and Table 2, it is shown that the DSC with the PVDF based polymeric gel electrolyte A shows a short-circuit current density (J_{sc}) of 14.89 mA cm^{-2}, an open-circuit voltage (V_{oc}) of 685 mV, fill factor (FF) of 0.74 and an energy conversion efficiency ($\acute{\eta}$) of 7.54%. When the LC was added into the PVDF based polymeric gel electrolyte, no obvious difference in the $V_{oc,}$ a decrease in *FF* and a remarkable increase (from 14.89 to 17.20 mA cm^{-2}) in the J_{sc} of the DSC were obtained yielding a relatively higher $\acute{\eta}$ (8.01%). The insert is the photocurrent action spectra of the DSC with electrolyte A and electrolyte B. The incident photon-to-collected electron conversion efficiencies (IPCE) of the DSC with electrolyte B exhibit a higher plateau of over 60% from 400 to 640 nm, reaching a maximum of 68% at 550 nm. And additionally, IPCE of the DSC with electrolyte B is always higher than that of the DSC with electrolyte A, which results in the higher $J_{sc.}$

Generally, when LC was added into the PVDF based polymeric gel electrolyte A the organic compound LC may absorb on the platinum electrode, which would decrease catalytic activity (see supplementary material) and consequently increase the series resistance of DSC. Besides relatively lower ion conductivity also contributes to the increase of the series resistance. Therefore the FF of the DSC with electrolyte B decreases (from 0.74 to 0.68)[32].

To illuminate the role of LC in the PVDF based polymeric gel electrolyte on the increase of J_{sc} of the DSC, research was first needed to confirm whether the J_{sc} was limited by the charge transport in electrolyte. Fig. 6 shows the dependence of photocurrent density at short circuit (J_{sc}) of the DSC with electrolytes on the illumination intensity (I). In the short circuit, the electron recombination in the dye-sensitized solar cells is generally considered to be negligible. From Fig. 6, it is shown that both J_{sc} are linearly proportional to illumination intensity, implying that photocurrent is not limited by the diffusion of iodide and tri-iodide redox species in the electrolytes. Although the introduction of LC into the PVDF based polymeric electrolyte would hinder the charge transport in the electrolyte, it still could fulfill the requirements of J_{sc} for the DSC. Moreover, at a given I, the J_{sc} of the DSC with electrolyte B is always higher than that with PVDF based polymeric gel electrolyte A.

Table 2
Photovoltaic performance parameters of dye-sensitized solar cells based on different electrolytes.[a]

Electrolyte	V_{oc} (mV)	J_{sc} (mA cm^{-2})	FF	$\acute{\eta}$ (%)
PVDF (A)	685	14.89	0.74	7.54
PVDF + LC (B)	685	17.20	0.68	8.01

[a] Measured at 25 °C.

As reported previously [33], J_{sc} can be calculated by integrating the product of the incident photo flux density and the cell's IPCE over wavelength used for light absorption by the dye, with the assumption that the potential drop by series resistance in the cell is negligible, the J_{sc} is shown as follows,

$$J_{sc} = \int qF(\lambda)[1 - r(\lambda)]\mathrm{IPCE}(\lambda)\mathrm{d}\lambda \quad (7)$$

where q is the electron charge, $F(\lambda)$ is the incident photo flux density at wavelength λ, and $r(\lambda)$ is the incident light loss before reaching the TiO_2 film in the cell. The IPCE is expressed as [34]

$$\mathrm{IPCE}(\lambda) = \mathrm{LHE}(\lambda)\phi_{inj}\eta_c \quad (8)$$

where (λ) is the light harvesting efficiency, ϕ_{inj} is the quantum yield of charge injection and η_c is the efficiency of collecting the injected charge at the back contact. It is believed that ϕ_{inj} is determined by the difference between excited state level and Fermi level of the semiconductor TiO_2, and η_c is related to the property of the TiO_2 thin film. So both ϕ_{in} and η_c have nothing to do with the electrolyte. Besides the $\phi(\lambda)_{ET}$ defined as electron-transfer yield (that is, the product of electron injection yield and charge collection efficiency) has been found to be close to 1 in the optimized high-efficiency DSC [33,35–37]. Therefore, the higher IPCE values of the DSC with electrolyte B may be caused by the increase of the LHE(λ). According to the previous report [32], the LHE(λ) of the cell depends heavily on (1) the properties of the dye, such as extinction coefficient, absorbance, and (2) the optical path length within the electrodes. Thus LHE(λ) is mainly increased by the increasing optical path of the incident light without considering the effect of dye. Tachibana et al. [33] investigated the light scattering properties of the TiO_2 films in detail based on the simplified two-flux model theoretically developed by Kubelka and Munk. They used the optical thickness $\sigma(\lambda)$ to consider the light scattering magnitude of the TiO_2 films, because $\sigma(\lambda)$ is widely accepted as an indication of the light scattering efficiency through the medium. In the same manner, we also adopted the optical thickness to characterize the light scattering property of the electrolyte qualitatively. The transmittance and diffused reflectance of the electrolytes were obtained through the sample configuration shown in Fig. 7a by integrating sphere (shown in Fig. 8). From Fig. 8, it is found that the diffused reflectance of electrolyte B is much higher than that of PVDF based polymeric gel electrolyte A, indicating that the introduction of LC would increase the light scattering efficiency. So it is suggested that the light trapping scheme is formed in the electrolyte B due to the

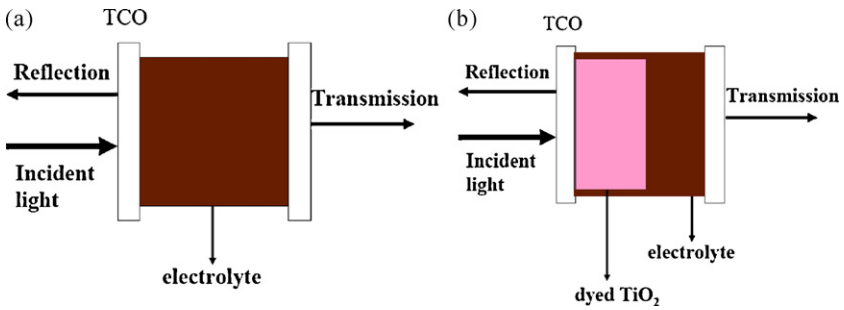

Fig. 7. Illustration of the configuration employed to measure the diffused reflectance and transmittance of the electrolyte (a), and transmittance of the DSC with different electrolytes.

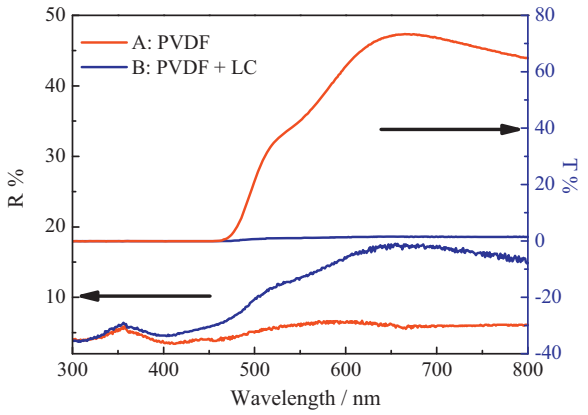

Fig. 8. The diffused reflectance and transmittance of the electrolytes.

addition of LC. Additionally, due to the light trapping scheme in electrolyte B, the light transmittance is also dramatically decreased (Fig. 8).

For the electrolyte, the optical thickness can be calculated from the following equation,

$$\sigma(\lambda) = \frac{R(\lambda)}{T(\lambda)} \tag{9}$$

where $R(\lambda)$ is the reflectance of the electrolyte, $T(\lambda)$ is the transmittance of the electrolyte. It is obvious that $\sigma(\lambda)$ of the electrolyte B is much higher than that of the PVDF based polymeric gel electrolyte A qualitatively, which would enhance optical path [32,33,38] and consequently the light harvesting efficiency.

Further support is obtained from the transmittance of the DSC (shown in Fig. 7b) with different electrolytes (Fig. 9). It is shown that

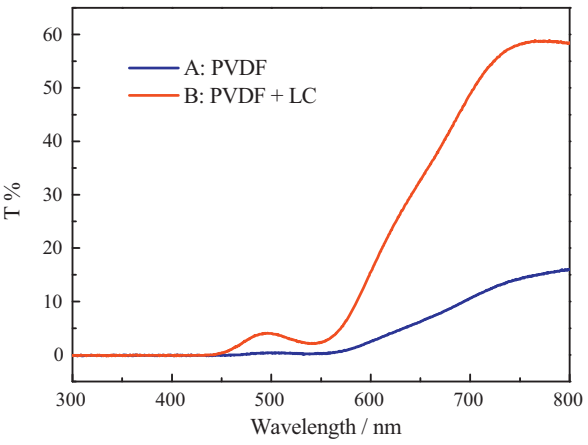

Fig. 9. The transmittance of the DSC with different electrolytes.

the transmittance of the DSC with electrolyte B is lower than that with PVDF based polymeric gel electrolyte A especially in the long wavelength region due to the existence of light trapping scheme, indicating that the incident light absorption by the dye of the DSC with electrolyte B was dramatically increased comparing with that of the DSC with PVDF based polymeric gel electrolyte A.

For the DSC with PVDF based polymeric electrolyte, we have the following electron continual equation as reported previously [39–41]

$$\frac{\partial n}{\partial t} = D\frac{\partial^2 n}{\partial x^2} - \frac{n}{t} + \alpha I_0 e^{-\alpha x} \tag{10}$$

here D is the diffusion coefficient of electrons and t is the electron lifetime determined by back-reaction with I_3^-. I_0 is the incident photon flux corrected for reflection losses by FTO, and α is the absorption coefficient. α is determined by the extinction coefficient of the dye, the internal surface area, the fractional surface coverage of the dye, and light scattering.

When LC was introduced into the PVDF based polymeric electrolyte for DSC, the electron continual equation should be made minor revision:

$$\frac{\partial n}{\partial t} = D\frac{\partial^2 n}{\partial x^2} - \frac{n}{t} + \alpha(I_0 e^{-\alpha x} + I') \tag{11}$$

where I' means the increased incident photon flux caused by the light trapping scheme in the liquid crystal based electrolyte B (Fig. 10). In the DSC, due to the space between TiO_2 nanoparticles and the inhomogeneous dye distribution [42] a certain part of incident light transmitted through electrolyte and could not be absorbed by the dye. When the electrolyte with light trapping scheme is used, the incident loss decrease, which contributes to the generation of the photoelectron according to Eq. (11).

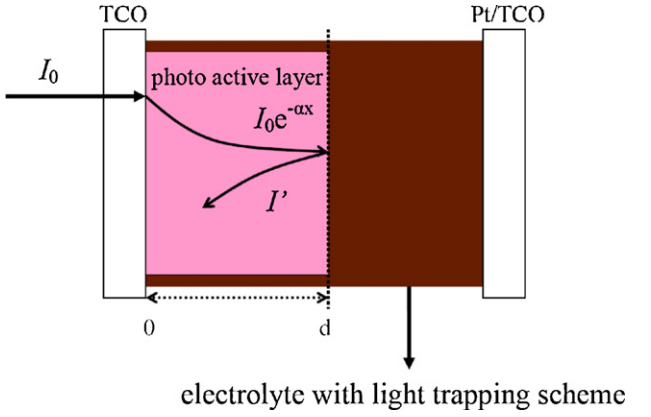

Fig. 10. Geometry for illumination of the dye-sensitized cell from the substrate side, showing the contribution of the electrolyte with light trapping scheme to dye absorption.

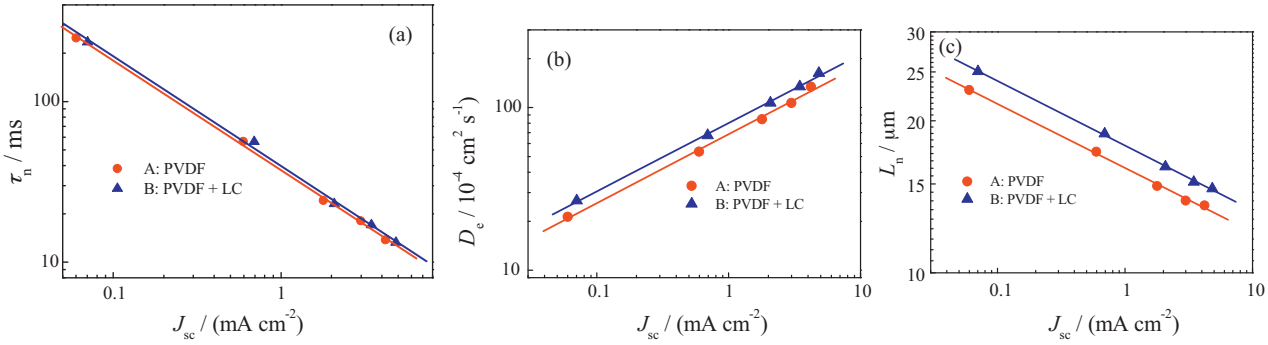

Fig. 11. Plots of (a) effective electron lifetime, (b) diffusion coefficient, and (c) diffusion length of the DSC with different electrolytes.

As reported, many studies focused on the light scattering property of the nematic LC [43–45] especially in the field of polymer dispersed liquid crystals (PDLCs)[16,46–48] containing the anisotropic LC molecules in the isotropic polymer matrix. Generally, when the LC was introduced into the polymer matrix, it forms micrometer-sized LC droplets filled with LC molecules and distributes randomly [49]. So when 4-Cyano-4′-n-heptyloxybiphenyl was embedded into the PVDF matrix, it may also form such droplets. And optical characteristics of such nematic droplets differ from those of the surrounding polymer matrix and the droplets can be viewed as optically anisotropic inhomogeneities [16], which scatter light incident upon them as confirmed above, that is to say, the light trapping scheme is formed in the electrolyte B. Therefore it would benefit the generation of the photoelectron.

Table 3 summarizes the photovoltaic performance parameters of DSC with different electrolytes at various illumination intensities. It is shown that the overall power conversion efficiencies are even higher under relatively low light intensity. More important, the conversion efficiency of the DSC with electrolyte B was only a bit higher than that of the DSC with PVDF based polymeric electrolyte under AM 1.5G sunlight (100 mW cm^{-2}). But, under a low intensity of 10 mW cm^{-2}, the conversion efficiency of the DSC with PVDF and LC based quasi-solid-state electrolyte B was raised by 17%, compared with the DSC with PVDF based polymeric gel electrolyte A.

3.3. Study of dynamic response of the DSC with different electrolytes by IMVS/IMPS

The intensity-modulated photovoltage spectroscopy [50,51] (IMVS) is always used to study the charge recombination at the TiO_2/electrolyte interface. IMVS measures the periodic photovoltage response of a testing cell to a small sinusoidal perturbation of light superimposed on a large steady background level, providing information on electron lifetime under open-circuit conditions.

Table 3
Photovoltaic performance parameters of dye-sensitized solar cells based on different electrolytes under different illumination intensity.

Light intensity (mW cm^{-2})	Electrolytes	V_{oc} (mV)	J_{sc} (mA cm^{-2})	FF	η (%)
110	PVDF (A)	685	16.38	0.73	7.44
	PVDF + LC (B)	686	18.92	0.67	7.91
100	PVDF (A)	685	14.89	0.74	7.54
	PVDF + LC (B)	685	17.20	0.68	8.01
58.4	PVDF (A)	670	8.69	0.75	7.47
	PVDF + LC (B)	667	10.04	0.72	8.26
31	PVDF	651	4.41	0.76	7.03
	PVDF + LC (B)	650	5.15	0.74	7.99
10	PVDF (A)	618	1.44	0.75	6.67
	PVDF + LC (B)	621	1.70	0.74	7.81

Fig. 11a presents the plot of electron lifetime versus J_{sc} which is linearly related to incident light intensity in the DSC with different electrolytes. It is obvious that, when the light intensity increases, the recombination becomes faster due to the higher electron concentration in the TiO_2 film. And the electron lifetime of the DSC with different electrolyte is very similar, implying no obvious difference in the V_{oc}. Intensity-modulated photocurrent spectroscopy (IMPS) [41,52], employing the same light perturbation and measuring the periodic photocurrent response, is used to study the charge transport under short-circuit conditions. Fig. 11b shows the plot of electron diffusion coefficient (D_e) versus J_{sc}. As the light intensity or the resultant J_{sc} increases, more deep traps will be filled with photoinjected electrons and do not retard the electron transport any more. The detrapping of electrons from shallow traps is much faster, resulting in a higher effective electron diffusion coefficient [53,54]. The electron diffusion coefficient of the DSC with electrolyte B is higher than that with electrolyte A due to the higher concentration of photoinjected electrons caused by the light trapping scheme in electrolyte B. The values of electron diffusion coefficient and lifetime can be used for the calculation of relative electron diffusion length (L_n) (shown in Fig. 11c), which is determined by the competition between electron transport and back reaction. Overall, the large electron diffusion length (L_n) directly related to a high charge collection yield is well consistent with the higher J_{sc} of the DSC with electrolyte B.

3.4. At-rest long-term stability of DSC with different electrolytes

Fig. 12 shows the comparison photoelectric conversion efficiency evolution of DSC with different electrolytes within time. After 1000 h, the efficiency of DSC with PVDF based polymeric gel

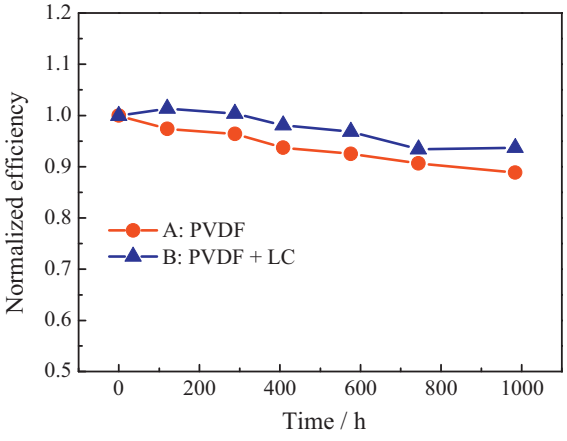

Fig. 12. The evolution of photoelectric conversion efficiency of different electrolytes based DSC with time.

electrolyte A retain over 88% of its initial value. While efficiency of DSC with electrolyte B retains over 92% of its initial value, indicating that When LC was introduced into PVDF based polymeric gel electrolyte A, the DSC exhibits relatively better stability. This may be associated with the higher boiling point of LC.

4. Conclusions

In summary, for the first time, the nematic liquid crystal, 4-Cyano-4′-n-heptyloxybiphenyl, was introduced into the PVDF based polymeric gel electrolyte for the DSC. The effects of addition of LC into the PVDF based polymeric electrolyte on the conductivity, ion diffusion, photovoltaic performance as well as dynamic response of the DSC were tested. Although the introduction of LC would hinder the mobility of the ions and decrease the conductivity and diffusion of tri-iodide and iodide, it still benefits the photovoltaic performance of the DSC due to the effective formation of light trapping scheme caused by the addition of liquid crystal. The optical thickness was extended to character the light scattering property of the electrolyte qualitatively. Due to the light trapping scheme formed by the addition of LC, the optical path of incident light is enhanced and consequently the light harvesting efficiency, which benefit the generation of photoelectron. Therefore the electron diffusion coefficients and diffusion length of the DSC were enlarged as well as photocurrent density, which offsets the lower fill factor and results in higher photoelectric conversion efficiency. Moreover, the at-rest stability tests show that when LC was added into PVDF based polymeric gel electrolyte, DSC could retain over 92% of its initial photoelectric conversion efficiency value after 1000 h. Further investigation about microstructure and light scattering property of this kind of quasi-solid-state electrolyte are in process.

Supplementary information

Photovoltaic performance parameters of DSC with different electrolytes and different dyes, photocurrent action spectra, *J–V* curves, photovoltaic performance parameters of DSC with liquid electrolyte, PVDF based polymeric gel electrolyte A and electrolyte B, analysis of the reduction of I_3^- at the platinum electrode with different electrolytes can be found.

Acknowledgment

This work was financially supported by the National Basic Research Program of China under grant no. 2011CB201600, the National High Technology Research and Development Program of China under grant no. 2009AA050603, Funds of the Chinese Academy of Sciences for Key Topics in Innovation Engineering under grant no. KGCX2-YW-326, and the Knowledge Innovation Program of the Chinese Academy of Sciences no. 075FCQ0125. We were also grateful to Dr. Peng Wang worked at Chang Chun Institute of Applied Chemistry Chinese Academy of Sciences for providing the C106 dye.

Appendix A. Supplementary data

Supplementary data associated with this article can be found, in the online version, at doi:10.1016/j.jpowsour.2011.02.051.

References

[1] B. Oregan, M. Grätzel, Nature 353 (1991) 737–740.
[2] M Grätzel, J. Photochem. Photobiol A: Chem. 164 (2004) 3–14.
[3] Y.M. Cao, Y. Bai, Q.J. Yu, Y.M. Cheng, S. Liu, D. Shi, F.F. Gao, P. Wang, J. Phys. Chem. C 113 (2009) 6290–6297.
[4] M.K. Nazeeruddin, F. De Angelis, S. Fantacci, A. Selloni, G. Viscardi, P. Liska, S. Ito, B. Takeru, M.G. Gratzel, J. Am. Chem. Soc. 127 (2005) 16835–16847.
[5] H.X. Wang, H. Li, B.F. Xue, Z.X. Wang, Q.B. Meng, L.Q. Chen, J. Am. Chem. Soc. 127 (2005) 6394–6401.
[6] P. Wang, S.M. Zakeeruddin, J.E. Moser, M. Grätzel, J. Phys. Chem. B 107 (2003) 13280–13285.
[7] U. Bach, D. Lupo, P. Comte, J.E. Moser, F. Weissortel, J. Salbeck, H. Spreitzer, M. Grätzel, Nature 395 (1998) 583–585.
[8] B. Bhattacharya, J.Y. Lee, J. Geng, H.T. Jung, J.K. Park, Langmuir 25 (2009) 3276–3281.
[9] W. Kubo, K. Murakoshi, T. Kitamura, S. Yoshida, M. Haruki, K. Hanabusa, H. Shirai, Y. Wada, S. Yanagida, J. Phys. Chem. B 105 (2001) 12809–12815.
[10] F.J. Li, F.Y. Cheng, J.F. Shi, F.S. Cai, M. Liang, J. Chen, J. Power Sources 165 (2007) 911–915.
[11] Y. Yang, C.H. Zhou, S. Xu, H. Hu, B.L. Chen, J. Zhang, S.J. Wu, W. Liu, X.Z. Zhao, J. Power Sources 185 (2008) 1492–1498.
[12] P. Wang, S.M. Zakeeruddin, J.E. Moser, M.K. Nazeeruddin, T. Sekiguchi, M. Grätzel, Nat. Mater. 2 (2003) 402–407.
[13] K. Binnemans, Chem. Rev. 105 (2005) 4148–4204.
[14] R.G. Weiss, Tetrahedron 44 (1988) 3413–3475.
[15] C.F.J. Faul, M. Antonietti, Adv. Mater. 15 (2003) 673–683.
[16] A.D. Kiselev, O.V. Yaroshchuk, L. Dolgov, J. Phys.: Condens. Matter 16 (2004) 7183–7197.
[17] N. Yamanaka, R. Kawano, W. Kubo, N. Masaki, T. Kitamura, Y. Wada, M. Watanabe, S. Yanagida, J. Phys. Chem. B 111 (2007) 4763–4769.
[18] R. Kawano, M.K. Nazeeruddin, A. Sato, M. Grätzel, M. Watanabe, Electrochem. Commun. 9 (2007) 1134–1138.
[19] S.C. Kim, M. Song, T.I. Ryu, M.J. Lee, S.H. Jin, Y.S. Gal, H.K. Kim, G.D. Lee, Y.S. Kang, Macromol. Chem. Phys. 210 (2009) 1844–1850.
[20] H.K. Kim, M.J. Lee, S.H. Jin, G.D. Lee, Mol. Cryst. Liq. Cryst. 510 (2009) 323–328.
[21] S.Y. Dai, K.J. Wang, J. Weng, Y.F. Sui, Y. Huang, S.F. Xiao, S.H. Chen, L.H. Hu, F.T. Kong, X. Pan, C.W. Shi, L. Guo, Sol. Energy Mater. Sol. Cells 85 (2005) 447–455.
[22] S. Dai, J. Weng, Y.F. Sui, C.W. Shi, Y. Huang, S.H. Chen, X. Pan, X.Q. Fang, L.H. Hu, F.T. Kong, K.J. Wang, Sol. Energy Mater. Sol. Cells 84 (2004) 125–133.
[23] L.H. Hu, S.Y. Dai, J. Weng, S.F. Xiao, Y.F. Sui, Y. Huang, S.H. Chen, F.T. Kong, X. Pan, L.Y. Liang, K.J. Wang, J. Phys. Chem. B 111 (2007) 358–362.
[24] Z.P. Huo, S.Y. Dai, C.G. Zhang, F.T. Kong, X.Q. Fang, L. Guo, W.Q. Liu, L.H. Hu, X. Pan, K.J. Wang, J. Phys. Chem. B 112 (2008) 12927–12933.
[25] Y. Yang, C.H. Zhou, S. Xu, J. Zhang, S.J. Wu, H. Hu, B.L. Chen, Q.D. Tai, Z.H. Sun, W. Liu, X.Z. Zhao, Nanotechnology 20 (2009) 10.
[26] M. Wang, X. Yin, X.R. Mao, X.W. Zhou, Z.Z. Yang, X.P. Li, Y. Lin, J. Photochem. Photobiol A: Chem. 194 (2008) 20–26.
[27] G. Vijayakumar, M.J. Lee, M. Song, S.H. Jin, J.W. Lee, C.W. Lee, Y.S. Gal, H.J. Shim, Y. Kang, G.W. Lee, K. Kim, N.G. Park, S. Kim, Macromol. Res. 17 (2009) 963–968.
[28] D.M. Li, M.Y. Wang, J.F. Wu, Q.X. Zhang, Y.H. Luo, Z.X. Yu, Q.B. Meng, Z.J. Wu, Langmuir 25 (2009) 4808–4814.
[29] K.M. Lee, V. Suryanarayanan, K.C. Ho, J. Photochem. photobio A: chem. 207 (2009) 224–230.
[30] P. Wang, S.M. Zakeeruddin, P. Comte, I. Exnar, M. Grätzel, J. Am. Chem. Soc. 125 (2003) 1166–1167.
[31] P. Wang, S.M. Zakeeruddin, I. Exnar, M. Grätzel, Chem. Commun. (2002) 2972–2973.
[32] N. Koide, A. Islam, Y. Chiba, L.Y. Han, J. Photochem. photobio A: chem. 182 (2006) 296–305.
[33] Y. Tachibana, K. Hara, K. Sayama, H. Arakawa, Chem. Mater. 14 (2002) 2527–2535.
[34] M.K. Nazeeruddin, A. Kay, I. Rodicio, R. Humphrybaker, E. Muller, P. Liska, N. Vlachopoulos, M. Grätzel, J. Am. Chem. Soc. 115 (1993) 6382–6390.
[35] J.S. Salafsky, W.H. Lubberhuizen, E. van Faassen, R.E.I. Schropp, J. Phys. Chem. B 102 (1998) 766–769.
[36] R. Katoh, A. Furube, T. Yoshihara, K. Hara, G. Fujihashi, S. Takano, S. Murata, H. Arakawa, M. Tachiya, J. Phys. Chem. B 108 (2004) 4818–4822.
[37] T.W. Hamann, R.A. Jensen, A.B.F. Martinson, H. Van Ryswyk, J.T. Hupp, Energy Environ. Sci. 1 (2008) 66–78.
[38] M. Zeman, R.A.C.M.M. van Swaaij, J.W. Metselaar, R.E.I. Schropp, J. Appl. Phys. 88 (2000) 6436–6443.
[39] G. Schlichthorl, S.Y. Huang, J. Sprague, A.J. Frank, J. Phys. Chem. B 101 (1997) 8141–8155.
[40] S. Sodergren, A. Hagfeldt, J. Olsson, S.E. Lindquist, J. Phys. Chem. 98 (1994) 5552–5556.
[41] L. Dloczik, O. Ileperuma, I. Lauermann, L.M. Peter, E.A. Ponomarev, G. Redmond, N.J. Shaw, I. Uhlendorf, J. Phys. Chem. B 101 (1997) 10281–10289.
[42] G. Franco, L.M. Peter, E.A. Ponomarev, Electrochem. Commun. 1 (1999) 61–64.
[43] S. Stallinga, M.M. Wittebrood, D.H. Luijendijk, T. Rasing, Phys. Rev. E 53 (1996) 6085–6092.
[44] L.M. Blinov, JETP Lett. 88 (2008) 160–163.
[45] Y. Utsumi, D. Kajita, S. Takeda, H. Kagawa, I. Hiyama, Y. Tomioka, K. Ono, Jpn. J. Appl. Phys. 47 (2008) 2205–2208.

[46] J.H.M. Neijzen, H.M.J. Boots, F.A.M.A. Paulissen, M.B. vanderMark, H.J. Cornelissen, Liq. Cryst. 22 (1997) 255–264.
[47] W.B. Li, H. Cao, M. Kashima, F. Liu, Z.H. Cheng, Z. Yang, S.Q. Zhu, H. Yang, J. Polym. Sci. Polym. Phys. 46 (2008) 2090–2099.
[48] N. Mizoshita, Y. Suzuki, K. Kishimoto, K. Hanabusa, T. Kato, J. Mater. Chem. 12 (2002) 2197–2201.
[49] E.E. Kriezis, Microw. Opt. Technol. Lett. 35 (2002) 437–441.
[50] N.G. Park, G. Schlichthorl, J. van de Lagemaat, H.M. Cheong, A. Mascarenhas, A.J. Frank, J. Phys. Chem. B 103 (1999) 3308–3314.
[51] G. Schlichthorl, N.G. Park, A.J. Frank, J. Phys. Chem. B 103 (1999) 782–791.
[52] J. van de Lagemaat, A.J. Frank, J. Phys. Chem. B 104 (2000) 4292–4294.
[53] J. Nelson, S.A. Haque, D.R. Klug, J.R. Durrant, Phys. Rev. B 63 (2001) 205321–205329.
[54] D. Shi, N. Pootrakulchote, R.Z. Li, J. Guo, Y. Wang, S.M. Zakeeruddin, M. Grätzel, P. Wang, J. Phys. Chem. C 112 (2008) 17046–17050.